Iraqi Geological Journal

Journal homepage: https://www.igj-iraq.org

Geohistory Model and Structural Style for Hydrocarbon Trapping Mechanism in Kendal Sub-basin, North Central Java, Indonesia

Sulistiyono[1,2*], Yoga Andriana Sendjaja[1], Abdurrokhim[1], and Billy G. Adhiperdana[1]

[1] Faculty of Geological Engineering, Padjadjaran University, Bandung, Indonesia
[2] Bandung Polytechnic of Energy and Mine, Indonesia
* **Correspondence**: sulistiyono22001@mail.unpad.ac.id

Received:
5 February 2025
Accepted:
12 May 2025
Published:
31 July 2025

Abstract

The geological complexity of the Kendal Sub-basin is strongly influenced by tectonic processes. These tectonic phases shape the basin's geometry, structural style, and depositional sequences. Structural features contribute to oil seepage manifestations, making this area a promising target for hydrocarbon exploration. This study aims to model the geological history and analyze structural controls on hydrocarbon trapping. The methods used are surface and subsurface geological structure analysis, including recording surface geological structures, fault fracture density analysis, identifying markers from well data, seismic interpretation, subsurface mapping, and making geological history models. Three tectonic phases influence the structural patterns in the Kendal Sub-basin. Beginning in the Early to Middle Miocene, rifting produced a half-graben. The Middle Miocene to Late Miocene north-south compression stage follows this. Finally, the Late Miocene to Late Pliocene fault stage as compression intensity increases, creates a thrust fold zone. The modelling of geological history is closely associated with the hydrocarbon trapping mechanism. Hydrocarbon generation occurs in the organic-rich Lower Cibulakan shale, with vertical migration through fault systems and lateral migration via rock pores until it is trapped in reservoir formations. This migration ceases once the hydrocarbon becomes trapped in the reservoir rock. The study identifies two primary trap types: structural traps (e.g., thrust anticline, sub-thrust, horst block) and stratigraphic traps (e.g., pinch-out sand, built-up carbonate).

Keywords: Geohistory model; Structural style; Hydrocarbon trapping; Kendal sub-basin

1. Introduction

The North Serayu Basin, located in North Central Java, extends from east to west, covering Kendal, Pekalongan, Pemalang, Tegal, and Brebes Regencies (Fig. 1). This basin is controlled by two major regional strike-slip faults: the Muria-Kebumen Sinistral Fault (Meratus Trend), trending southwest-northeast, and the Pamanukan-Cilacap Dextral Fault (Sumatran Trend), trending northwest-southeast. These faults result from the subduction of the Indian Plate beneath Java, producing a north-south compression trend of ellipsoids (Satyana, 2005). The geological structure of this basin is divided into three sub-basins: Kendal, Pemalang, and Tanjung Sub-basins. Exploration activity in the North Serayu Basin remains limited compared to the mature hydrocarbon-rich areas of West Java and East Java. The North West Java basin is very productive in discovering oil and gas fields, such as the Jatibarang, Offshore North West Java, Tambun, Eretan, and others. Likewise, with the North East Java Basin, such as Banyu Urip, Sukowati, Mudi, and others. The North West Java basin is said to be "terra

incognita", an area with geological conditions that are not well known in oil and gas exploration, so it still triggers the emergence of many different opinions regarding the geological conditions of the local area (Satyana, 2007). The Kendal Sub-basin, situated in the eastern part of the North Serayu Basin, is bordered to the south by the Dieng volcanic complex, Mount Sindoro, and Mount Sumbing. The sub-basin is characterized by three dominant structural trends: (1) thrust faults trending west-east and northwest-southeast, (2) normal faults trending northwest-southeast and west-east, and (3) left-slip faults trending northeast-southwest (Audithia et al., 2016). The northwest-southeast trending structure has a strike-slip fault mechanism that intersects the main fault, and other northeast-southwest trending strike-slip faults formed after the thrust fault (Jamal et al., 2024). Gravity modelling in the southern mountains and the Kendeng basin, the thrust fault belt shows a major fault with a steep slope facing south (Novianto et al., 2022).

Hydrocarbon exploration activities in the North Serayu Basin and its surroundings began in the late 1800s. The Dutch oil company has conducted exploration drilling in the Klantung Field southwest of Semarang City. This field produced 12 wells with a cumulative of 400 tons from 1903 to 1912. The highest production was achieved in 1933 by producing 107,000 barrels of oil from 28 development wells. In 1980 and 1982, Pertamina drilled the NCJ-A1 and NCJ-B1 wells with the status of gas discovery and were temporarily abandoned. Then, in 2005, the drilling of the KTG-1 well was continued with the status of a non-commercial oil discovery well. Oil seepage is also found in the Karangkobar, Bawang, Suban, Klantung, Sodjomerto, Kaliwaru, and the eastern and western parts of the Ungaran mountains. The manifestation of oil seepage occurred due to a Pliocene compression tectonic process with a North-South stress direction, resulting in folding and faulting as a migration route for hydrocarbons to the surface (Nursecha et al., 2014). Hydrocarbon seeps continue to spark debate among experts regarding the source rocks from which these hydrocarbons originate (Logan et al., 2010; Wang et al., 2024; Zhang et al., 2019). Geochemical analysis suggests that the hydrocarbons originated from thermally mature source rocks deposited in estuarine or shallow lacustrine environments (Praptisih, 2016).

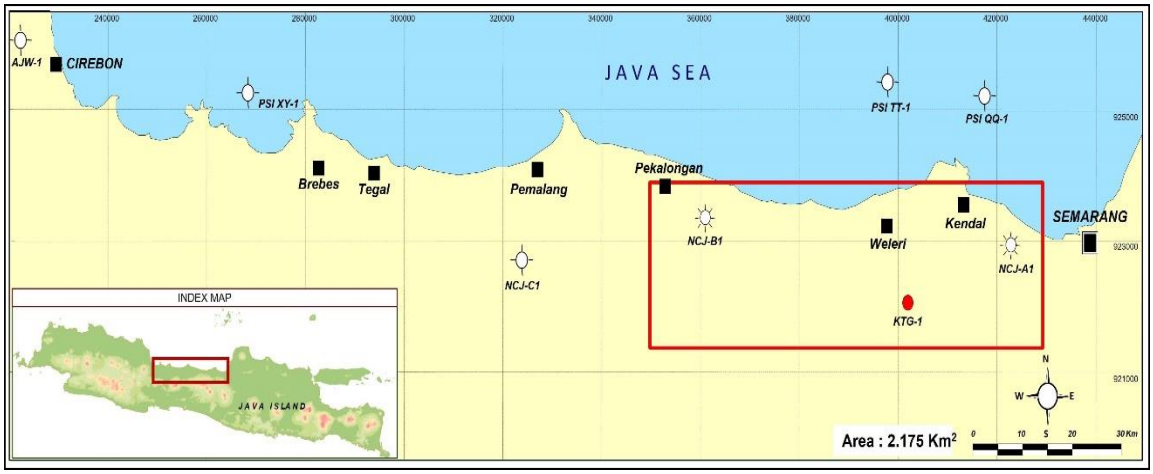


Fig. 1. Research location map. Located in the northern part of Central Java, covering Kendal and Pekalongan districts occupy an area of 2,175 square km

The structural geological conditions in the research area are very complex in the form of a thrust fold belt, so the understanding of the petroleum system is not yet well known. The thrust fold belt extends from the Sunda Strait to the Bali and Flores Basins and is referred to as the Baribis-Kendeng Fault (Simandjuntak and Barber, 1996). The Baribis Fault was identified in the northern part of West Java with a relative West-East alignment extending from Bekasi to Kuningan, which is known as the West Java Back-arc Thrust (WJBT) (Aribowo et al., 2022; Gunawan and Widiyantoro, 2019; Irsyam et

al., 2020; Pasari et al., 2021). This research aims to reconstruct the geological history of the Kendal sub-basin and analyze structural controls on hydrocarbon trapping. The study integrates surface and subsurface data to evaluate the basin's tectonic evolution and petroleum system. By identifying hydrocarbon traps, this study contributes to the broader understanding of hydrocarbon potential in underexplored areas of the Kendal Sub-basin. There has not been much research on structural control of the types of hydrocarbon traps that form in the research area.

2. Regional Geology

Kendal Sub-basin is located in the eastern part of the north Serayu basin. The physiography of the sub-basin is an east-west trending mountain range, with a curved geometry opening towards the south, and Quaternary volcanoes occupy both ends. The eastern end starts from the alignment of the Sumbing and Sindoro Mountains in a northwest-southeast direction, which continues with the presence of the Dieng volcanic complex in a west-northwest direction, and the presence of Mount Slamet marks the western part (Husein et al., 2013). Based on gravity analysis and geological structure alignment, Semarang Heights is interpreted as the boundary of the North Serayu Basin and the Kendeng Zone (Romario et al., 2016; Wilson and Hall, 2010). Tectonically, the Kendal Sub-basin formed as a result of rifting processes in the Middle Eocene, producing a northeast-southwest trending half-graben and a broad platform (Fig. 2). During the Early Miocene, there was a compression regime along with the northward subduction of the India-Australia Plate beneath the Eurasian Plate. This process was intensified again during the Pliocene-Pleistocene time, resulting in folding and causing inversion of the earlier graben. Sedimentation began during the Middle Eocene rifting process, along with the formation of half-graben and broad platforms with sedimentation of tertiary deposits. Along with the rifting process, volcaniclastic sedimentation from the equivalent of the Jatibarang Formation and Early Oligocene-Miocene sediments from the Lower Cibulakan were deposited. This formation is composed of lacustrine sediments, rich in organic matter, delta shale, and coal deposited in the graben area, resulting in good quality of source rock maturity. Graben areas act as clastic fairways, where sand-rich, fluvial-deltaic sediments provide excellent reservoir potential. Meanwhile, poor reservoir quality is found in places dominated by volcaniclastic facies. Meanwhile, thin sediments dominated by shale and shallow sea sand will be deposited on the platform, providing the quantity and quality of source rock and oil and gas reservoirs.

The oldest sedimentary rocks in the Kendal Sub-basin are dated to the Oligo-Early Miocene, equivalent to the Lower Cibulakan Formation. It comprises shale, sandstone, siltstone, and coal. Then, it was deposited in conformable with the upper Early Miocene sediments of the Middle Cibulakan Formation, equivalent to the lithology dominated by limestone. The Middle Miocene age sediments are aligned above the Early Miocene sediments, namely the Upper Cibulakan Formation Equivalent. Lithology generally comprises alternating shale, sandstone, siltstone, and limestone. Sedimentation continues with the deposition of lower Late Miocene sediments, equivalent to the Parigi Formation, consisting of reef limestone interbedded with clastic shale. Then, Late Miocene-Pliocene sediments were deposited in a conformable form on top of the lower Late Miocene sediments. These Miocene-Pliocene sediments are exposed around the Klantung area as the Kerek Formation. Based on stratigraphy, this formation is equivalent to the lower Cisubuh Formation, with the constituent lithology alternating between mudstone and sandstone, with a layer of clastic limestone found at the bottom (Adha, 2021). The Pliocene-Pleistocene compression phase, followed by erosion and tectonic activity, led to the formation of the Upper Cisubuh Formation.

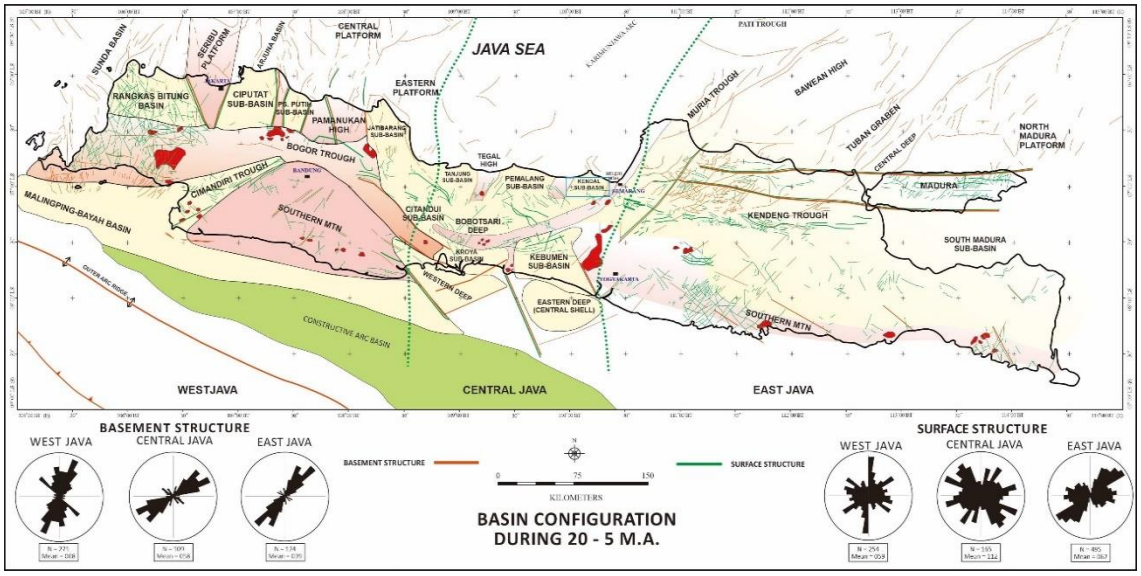


Fig. 2. Geological structure patterns of the island of Java. The North Serayu Basin is divided into Tanjung, Pemalang, and Kendal Sub-basins, with relative structural orientation trending northeast-southwest (Sribudiyani et al., 2003).

3. Materials and Methods

3.1. Materials

Seismic interpretation incorporates 60 seismic lines from three vintages (1980, 1982, 1998) with moderate to good data quality (Table 1). These data sets, along with well logs from NCJ-A1, NCJ-B1, and KTG-1, enable the identification of key stratigraphic markers and structural features (Fig. 3). The well contains logging data and reports on laboratory analysis results. Sub-surface seismic stratigraphic interpretation is supported by seismic attributes that focus on changes in lateral seismic facies and provide detailed information about the architecture of the sedimentary basins (Abd and Abd, 2023). The results of seismic interpretation and subsurface maps will be used to model the geological history and the forces influencing structural formation, enabling the identification of hydrocarbon trapping mechanisms in the study area. In addition, aerial photo data and geological maps are used in the fault fracture density (FFD) mapping process to determine high or low morphological density, which indicates the straightness of the surface geological structure. FFD is created based on straightness data in DEM (Digital Elevation Model) images and geological maps of the North Central Java area.

Table 1. Seismic data availability

Seismic ID	Seismic ID	Seismic ID	Seismic ID	Seismic ID	Seismic ID
80pkl-06-2033	80pkl-4b	80wlr-13	82btg-2a	98knd-06	98knd-17
80pkl-08a	80pkl-6-1447	80wlr-15a	82wlr-05a	98knd-07	98knd-19
80pkl-10a	80pkl-6-801	80wlr-17a	82wlr-08	98knd-08	98knd-21
80pkl-12a	80wlr-01	80wlr-4	82wlr-21	98knd-09	98knd-23
80pkl-15	80wlr-02	80wlr-9a	82wlr-7a	98knd-10	98knd-25
80pkl-17	80wlr-03	82btg-02	98knd-01	98knd-11	98knd-27
80pkl-19	80wlr-03a	82btg-03	98knd-02	98knd-12	98knd-29
80pkl-21	80wlr-05	82btg-04	98knd-03	98knd-13	98knd-31
80pkl-23	80wlr-06	82btg-05	98knd-04	98knd-14	98knd-10
80pkl-25	80wlr-11a	82btg-07	98knd-05	98knd-15	98knd-10a

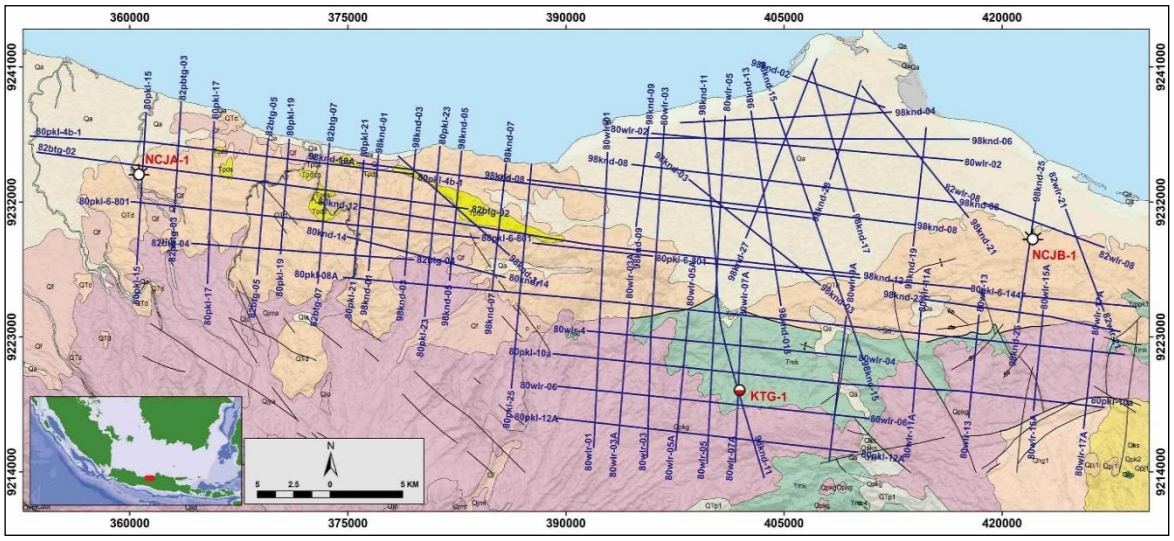


Fig. 3. Availability of seismic and well data in Kendal Sub-basin. The orientation of the seismic line is north-south and west-east, with relatively close distances between them

3.2. Methodology

The study employs a combination of field surveys and studio-based evaluations. Field surveys involve stratigraphic data collection, lithology sampling, structural measurements to determine fault kinematics, and FFD analysis. FFD analysis can help to interpret surface geological structure patterns. Studio evaluations focus on two key aspects: (1) regional geological and structural analysis and (2) subsurface data processing. These analyses are used as input for seismic interpretation and subsurface mapping combined with field survey results. The results of interpretation and subsurface mapping are used to create models of the geological history and forces that influence these structures to form, so that we will know about the hydrocarbon trapping mechanisms in this area (Fig. 4).

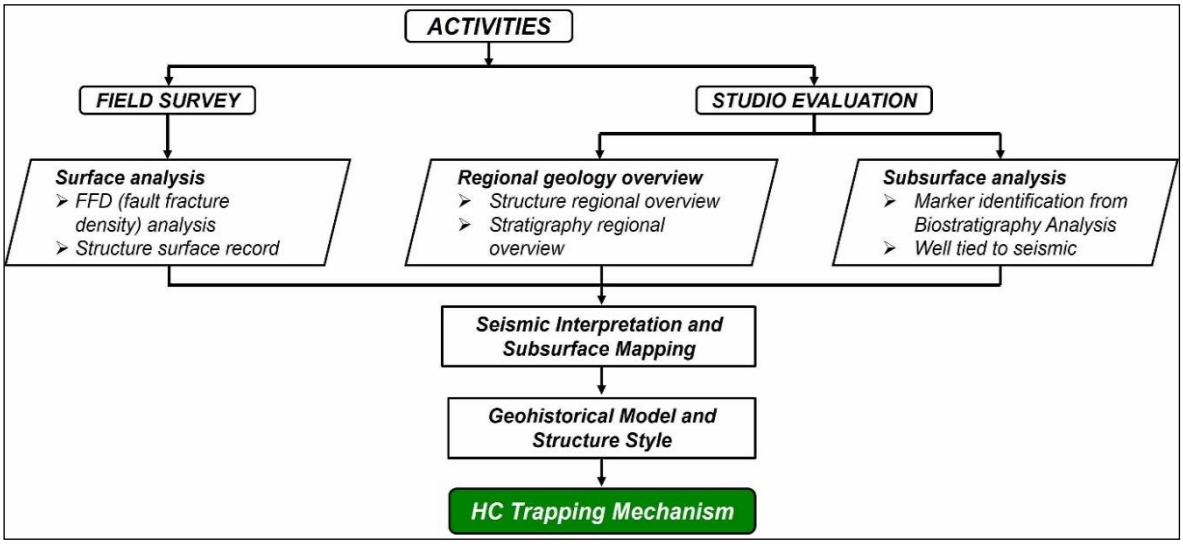


Fig. 4. The flow diagram of the research methodology with the scope of activities, in general, is field surveys and studio evaluations.

Field survey activities aim to collect surface geological data, including observation, measurement, and analysis of fault structural elements to interpret surface geological structures. In addition, samples of selected rocks were taken for laboratory analysis. The observations, results, and measurements of

structure surface data are intended to determine the kinematics of the main stresses. They are also used to validate the results of fault interpretation on subsurface data, which may continue to reach the surface. The results of the FFD method also reinforce the validation of subsurface geological structure patterns. This method assesses areas with high structural density caused by interconnected faults and fractures. The relationship between fault architecture (including antithetic faults, branch points, displacement gradients, and relay zones) and fracture density can help in understanding the complexity of the structure of the fracture development, thus affecting the quality of permeability in reservoir rocks (Camanni et al., 2021; Li et al., 2024). Lineaments are line structures that can be mapped from the surface and are a morphological expression of geological structures (Ângelo da Silva Neto et al., 2021; Heriawan et al., 2021; Majumdar and Bhattacharya, 1988; Meixner et al., 2018; Syaeful et al., 2024). These alignments include ridges, valleys, river flow patterns, and elevation contrasts. The direction of the lineaments obtained can also be interpreted as the main stress direction based on tectonic models (Harding, 1985).

The studio evaluation includes three activities: a preliminary study of a general overview of regional geology and a review of structure and stratigraphy. This stage is a literature study from previous authors regarding the geological conditions of the research area and its surroundings, which will assist in the analysis and evaluation process. The second activity is well data evaluation, including biostratigraphic analysis and chronostratigraphic correlation. Biostratigraphic analysis is in the form of reinterpretation of well data, which produces the geological age of rocks and depositional environment (Kurniasih et al., 2021; Sharaf and Sheikha, 2021; Zhu et al., 2025). The results of this analysis are in the form of determining the top marker in the well, which will later be used in the well and tied to the seismic data to obtain the position of the marker.

4. Results and Discussion

Forces and stresses influence the geometry, orientation, and type of geological structures that develop. This event will be reflected in surface and subsurface data in folding and faulting. The consequences of this process will influence the configuration and sedimentation at each age of deposition. Geological history modelling can track the development of geological structure and sedimentation at each age event. It will have implications for the petroleum system model in the research area. This will be discussed in more detail by discussing the condition of the surface and subsurface geological structures, geological history, and structural styles, as well as the implications for the hydrocarbon trapping mechanism.

4.1. Surface Geological Structure

Identification of surface geological structures is carried out using two approaches: interpreting aerial photo data using the FFD method and measuring geological structural elements in the form of faults, joints, and folds in the field.

4.1.1. Fault fracture density analysis

Based on the FFD map, the study area has varying density values ranging from low density (green colour) to high density (red colour). The relatively high density is distributed in the southern part of the study area. This event is a structure dominated by high hills and fault scarps. A high-density value interprets the intensive structure by indicating weak zones and a high level of good permeability (Alencar et al., 2024; Badawi and Gildin, 2025; Giao et al., 2025; Mendes et al., 2024). Areas with high-density values are interpreted as associated with regional geological structures (Thaden et al., 1975). The FFD interpretation results in faults and escarpments that emerge to the surface with high density. Meanwhile, a low-density value indicates a low morphology (denudational area). Low-density

areas are relatively unassociated, and it is impossible to find structures that occupy the northern part of an alluvial plain. Based on the delineation of structural lineaments, the research area is dominated by the west-east and northwest-southeast regions. The main thrust is interpreted to be north-south or perpendicular to the lineament direction (Fig. 5).

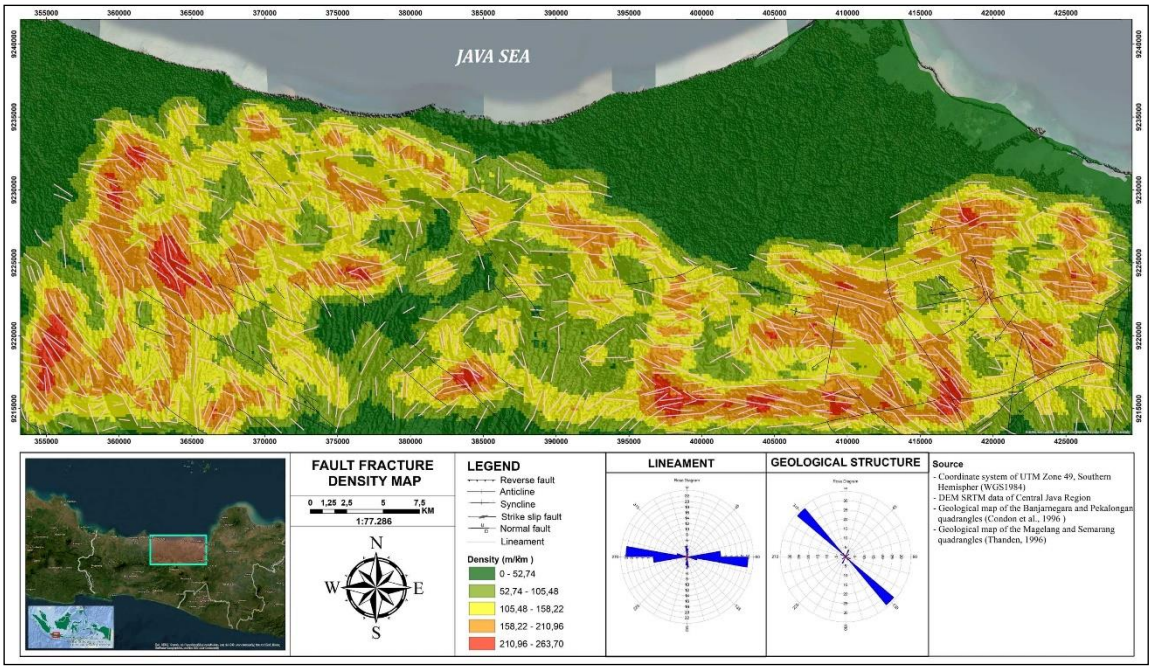


Fig. 5. Kendal Sub-basin fault fracture density map. High density (red) indicates intensive structures with indications of fault zones and high levels of permeability. The west-east and northwest-southeast directions dominate the direction of the structure's alignment

4.1.2. Surface structure record

Geological structures in faults, fractures, and folds are found at several outcrops in the research area. This structure is often found in the Sojomerto area, Kendal Regency, along the river that cuts through the Lower Cisubuh Formation (Fig. 6 and 7).

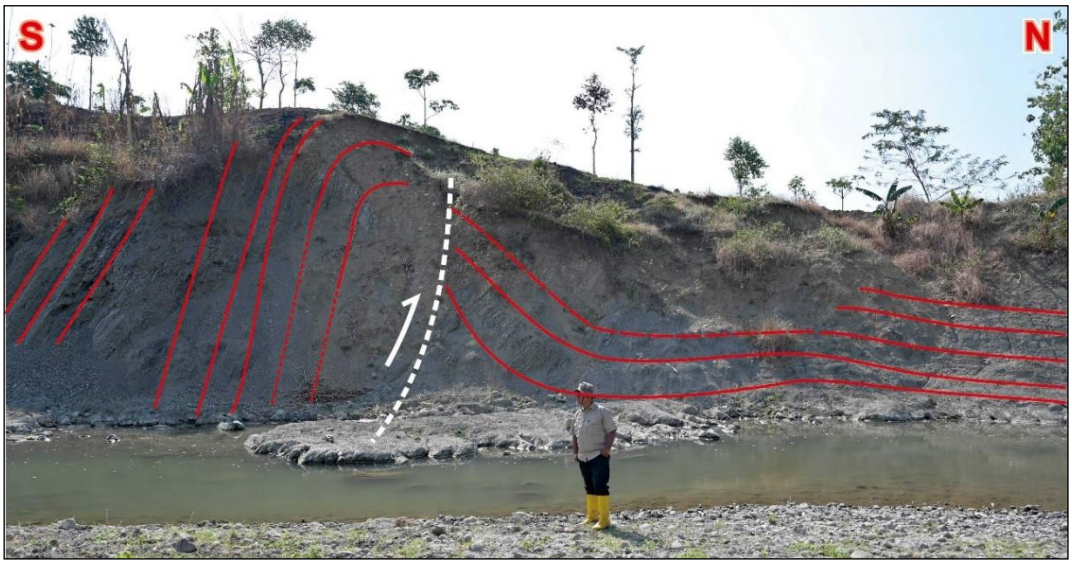


Fig. 6. The appearance of a thrust fault in the Seneng River, Sojomerto, Kendal Regency. Asymmetric folding with vertical layer angles on the south flank and even thrust faults with the hanging wall section on the south side. (camera facing west)

This formation is well-exposed and dominated by transgressive shale sediments. Folding accompanied by thrust faults was formed due to compressive forces during the Pliocene-Pleistocene period. Thrust faults are assumed to have a continuous decollement down to the base. The field's fold and fault structure analysis shows the folding direction is relatively north-south, with the southern flank's steeper angle at an almost vertical angle of 75º. The folding top has shifted with the hanging wall position in the south and has a west-east alignment (N 110 E). Apart from discovering folds and faults in the field, many morphological forms of fault slopes, straight ridges, and waterfalls were also found to indicate weak zones at this location. This morphological position is based on the interpretation of FFD discussed in the previous section.



Fig. 7. Thrust block faulting in the Seneng River, Sojomerto, Kendal Regency. (camera facing east)

4.2. Subsurface Evaluation

Subsurface geological evaluation determines basin configuration, trapping models, distribution patterns, and the geological structures vertically and laterally. Sixty seismic line data were used for subsurface analysis. The seismic lines are oriented predominantly in north-south, west-east, and, in some cases, northwest-southeast directions. The seismic data quality is generally classified as moderate to good, with reflector continuity being observable in all parts of the study area. This evaluation also used three exploration wells' data, including NCJ-A1, NCJ-B1, and KTG-1 Wells. Selected markers were interpreted based on seismic data, including basement, lower Cibulakan, middle Cibulakan, upper Cibulakan, Parigi, and Cisubuh. Marker determination is based on biostratigraphic data of rocks in Well NCJ-A1 and tectonic events that influence the sedimentation pattern of each marker (Fig. 8). Biostratigraphy in the form of rock age analysis and interpretation of the depositional environment. Meanwhile, tectonic events produce sea-level changes that control sedimentation sequences. NCJ-A1 well marker identification is used in the process of well tie to seismic (Fig. 9).

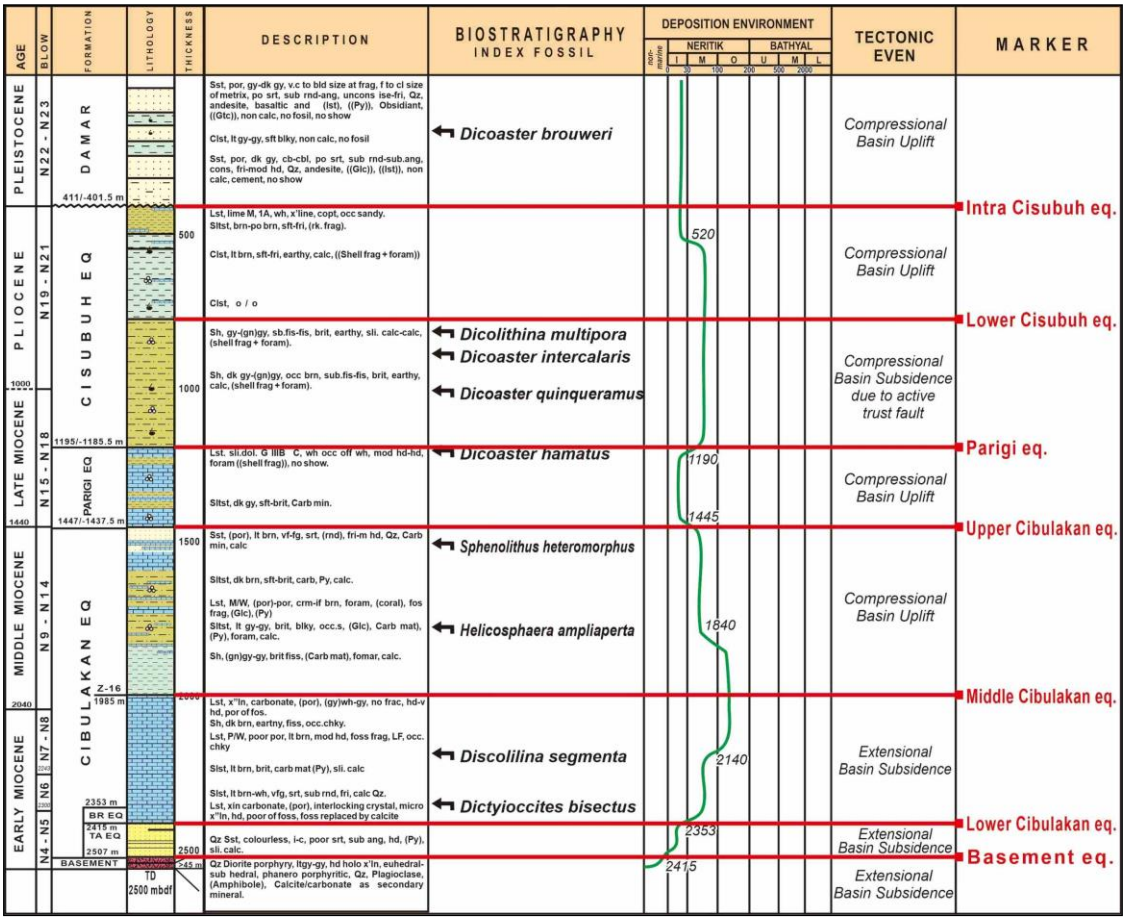


Fig. 8. Marker determination in Well NCJ-A1 based on biostratigraphic analysis and tectonic events

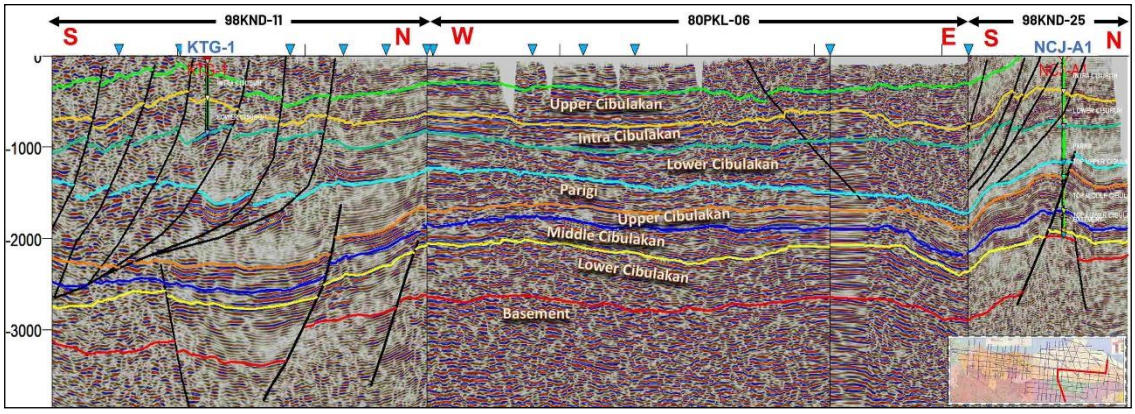


Fig. 9. Well-tied to seismic process in NCJ-A1 and KTG-1 Wells with marker distribution in the research area

4.2.1. Basement marker

The basement is the lowest marker that is interpreted in the research area. This marker is a reflection of the Kendal Sub-basin configuration. The depth of the basement marker in the NCJ-A1 well is 2,507 m or 1,979 ms on the seismic data. Seismic marker events are indicated by the difference in reflectors above and below the marker. A clear reflection characterizes the top of the marker, and its continuity can be followed.

In contrast, the bottom of the marker shows a brittle and random pattern (Fig. 10). This marker is cut by a normal fault block with displacement to the south due to the Oligo-Miocene tectonic extension phase. This normal fault block causes the sediments above the basement to thicken as syn-rift sediments. These normal faults will separate high and low areas with a relative northeast-southwest orientation. The relatively low structure is located in the south, extending from west to east, and is interpreted as where hydrocarbon is generated (Fig. 11).

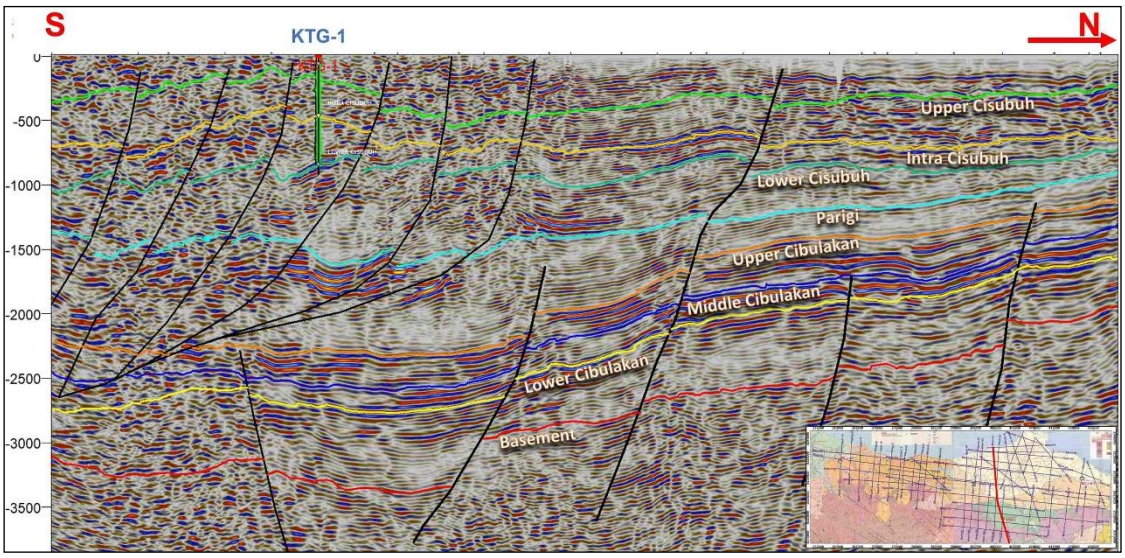


Fig. 10. The seismic interpretation of the 89knd-11 line is in a north-south direction. The geological structure is very complex due to tectonic influences from different stages of style and age, which will result in hydrocarbon trapping in the study area

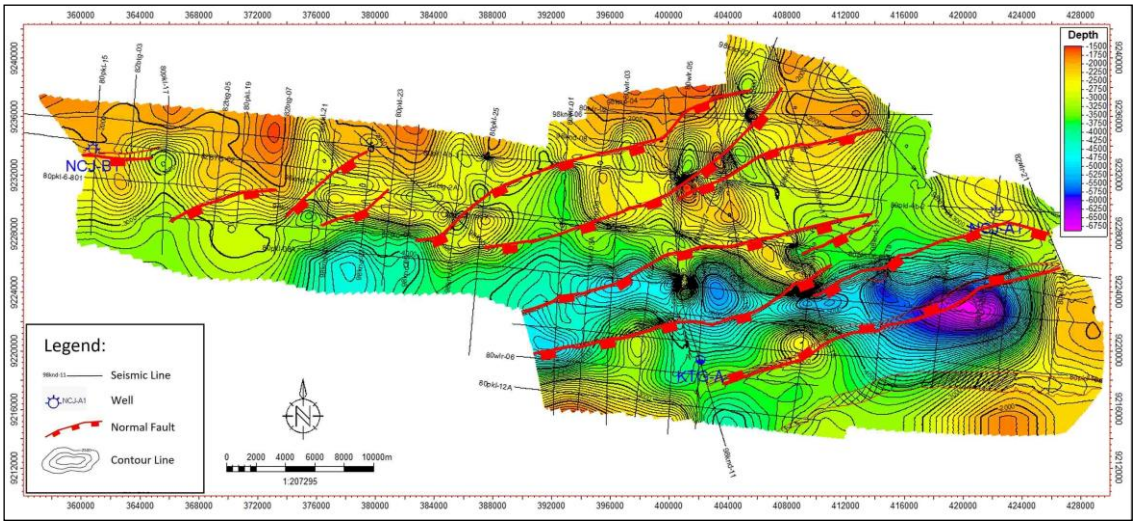


Fig. 11. Depth structure map of the basement marker with northeast-southwest fault orientation.

4.2.2. Lower cibulakan marker

This marker was deposited above the basement and extends across the research area. Strong reflector terminations characterize seismic marker events. The seismic peaking process is carried out on the "black peak" with varying layer thicknesses in several places. Thickening layers occupy the half-graben area, and normal fault movement occurs (can be seen in Fig. 10). This marker is a sedimentary syn-rift product with deposits on the sides by the fluvial-deltaic sandstone at the bottom and lacustrine shale at the top (Moura Costa et al., 2023; Nabawy et al., 2023; Xu and Ren, 2025). The fault

structure's geometric pattern still follows the basement model, trending northeast-southwest. Normal faults bound the high and low structures in a northeast-southwest direction. Based on the NCJ-A1 well, this marker was found at a depth of 2,415 m or in seismic data at 1,920 ms.

4.2.3. Middle cibulakan marker

The middle Cibulakan marker was deposited above the lower Cibulakan marker, with the constituent lithology dominated by limestone. Based on well NCJ-A1, this marker was encountered at a depth of 1,985 m. This marker was formed due to the peak of the transgression phase due to tectonic dragging that occurred during the Early Miocene. The seismic characteristics of this marker are characterized by a strong and continuous reflector with local appearances of mounded shape, wavy sub-parallel, chaotic, and downlap reflection as characteristics of a pinnacle reef (Betzler et al., 2024; Feng et al., 2017; Harzali et al., 2014) (can be seen in Fig. 10). Well tied to seismic results, this marker is at the reflector interface at "zero peaks". This marker is applied continuously in all research areas with a relatively constant thickness. The geometry of the normal fault structure is still seen cutting and following the pattern of the underlying marker with a lineament trending northeast-southwest (Fig. 12).

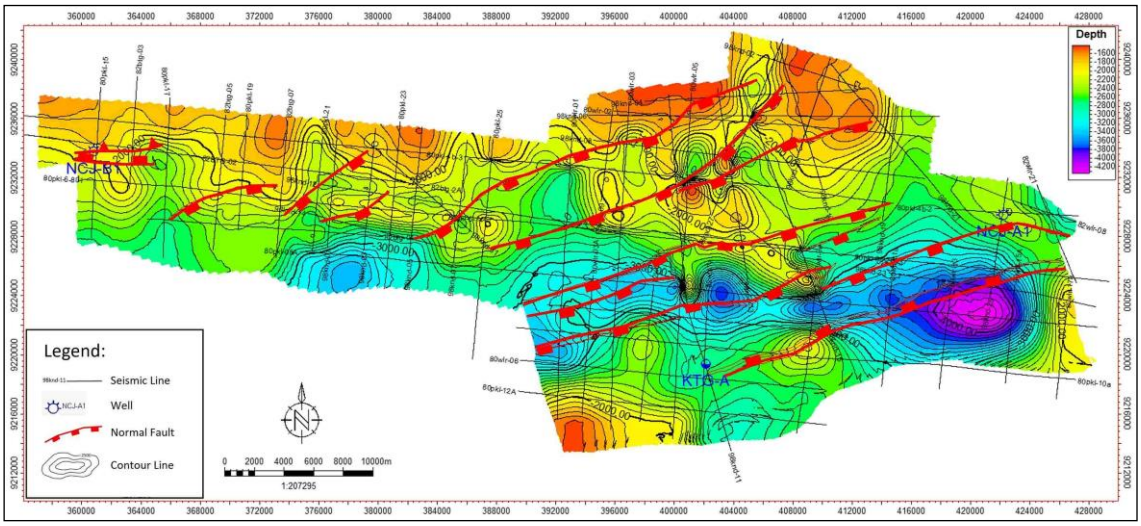


Fig. 12. Depth structure map of the middle Cibulakan Marker, which is the maximum limit of the flooding surface (FS) ending in the research area

4.2.4. Upper cibulakan marker

This marker was deposited conformably above the middle Cibulakan with an even sediment distribution pattern throughout the study area. Seismic data show that the reflector on this marker is characterized by parallel, strong, and continuous terminations (can be seen in Fig. 10). Well tied to seismic results, the marker is at the "black peak" reflector interface. This marker began to be influenced by compressional forces, resulting in the appearance of several traces of ascending faults and a Middle Miocene-aged fault slip layer. The relative fault orientation still follows the pattern of the northeast-southwest structure. Elevated structures are visible in the north and south and are bounded by a low in the centre. The subsurface geological mapping results show that this marker's deepest part is 2,495 m, while the shallowest part is 967 m.

4.2.5. Parigi marker

Compression forces still control the fault structure at this marker. As a result of intensive tectonics, the southern part of the study area undergoes uplift faulting in a northeast-southwest direction. The uplift structure formed is an anticline fold with the shifted northern flank and a continuous sliding plane

into one on the marker below. Based on the NCJ-A1 well data, Parigi Marker comprises clastic limestone lithology at the bottom and the pinnacle reef at the top. Parallel reflector types at the bottom characterize the seismic data, and in some places, mounded and chaotic at the top (can be seen in Fig. 10). The relatively high structures are in the northern and southern parts, with the shallowest depth at 741 m and the deepest in the middle with a depth of 2,116 m.

4.2.6. Cisubuh marker

Regionally, this marker is controlled by Pliocene-Pleistocene inversion tectonics, which activated old faults into folding and faulting. The dominant thrust fault structure is found at this level with a northeast-southwest orientation. This resulted in the formation of structural traps in the southern part of the study area. High areas dominate almost 2/3 of the study area spread across the north and south (Fig. 13). The low structure is relatively developed in the central part. Based on the NCJ-A1 well, the marker depth is 401.4 m or 378 ms on the seismic data. The seismic interpretation results show that this marker is characterized by a brittle and relatively discontinuous seismic reflector due to the thrust fault zone that occurred (can be seen in Fig. 10). This marker seismic trace is located at the "black peak" reflector interface with the distribution pattern assumed to be continuous throughout the study area.

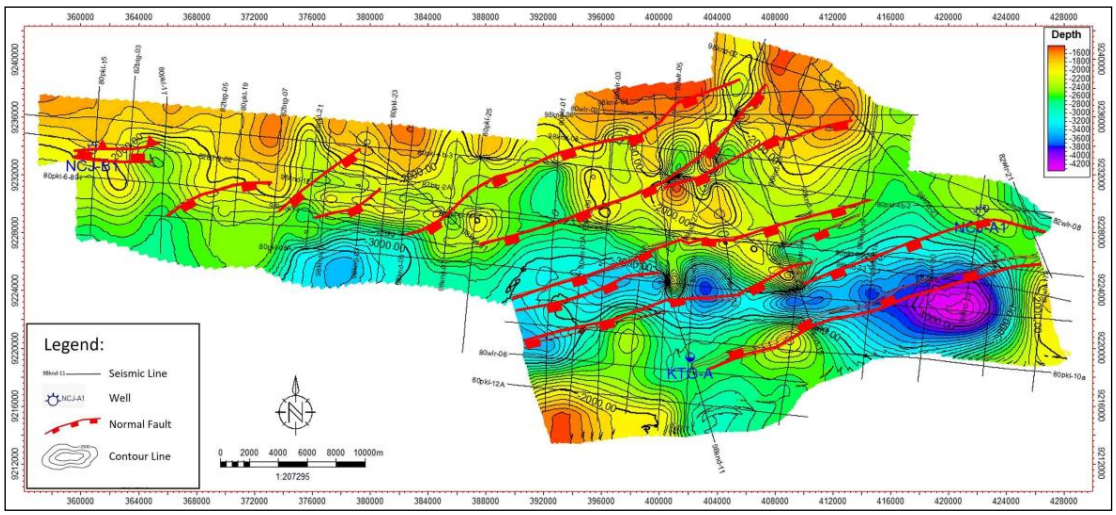


Fig. 13. Depth structure map of Cisubuh Marked controlled by thrust faults due to compression and the Plio-Pleistocene tectonic activation

The relationship between subsurface and surface geological structures can be observed in the continuity of fault and folding patterns. The geological structure at the Cisubuh Marker will extend to the surface in the form of fault events such as jointing, layer displacement, fault straightening, and morphological offset. The results of the mapping of the subsurface fault are relatively west-east. The orientation of this fault is adjusted to the straightness of the fault on the surface and the FFD map. Micro anticlines are also found in the Klantung Field as a continuation of the folding beneath the surface. This anticline structure is very ideal as an effective hydrocarbon trap in this field.

4.3. Geohistory Model and Structural Style

The results of the 98knd-11 seismic interpretation across the KTG-1 Well show continuous horizon overlay in all seismic sections. Based on the interpretation of seismic data on this track, three tectonic phases were identified that controlled the basin's development and greatly influenced the lithologic formation. The first tectonic phase has been recorded since the Early Miocene, which began with an extensional event until the Middle Miocene. Then, the second tectonic event was compressional in the

Late Miocene, and the last phase was an increase of compressional events in the Early Pliocene until the basin closed. Stratigraphic records from the analysis of the NCJ-A1 well and the development of geological structures from the interpretation of the 98knd-11 seismic trajectory can formulate the development of the basin evolution based on tectonic events (can be seen in Fig. 10).

4.3.1. Early Miocene-Middle Miocene

Starting from basement rocks (which are not well identified) that were formed in the nonmarine-inner neritic environment. The emergence of several major fault traces that cut through the basement is a precursor to the formation of normal faults due to the extensional phase. This phase will produce high and low areas that allow for the deposition of sedimentary rocks (Fig. 14a). Then, superimposed on the basement is the Lower Cibulakan Marker deposited in the inner neritic environment. This sediment results from the syn-rift phase in the form of normal block faulting with sediment filling in the half-graben (Fig. 14b). Based on the lithology of the NCJ-A1 well, this deposit is dominated by terrestrial sediments, including poorly to moderately sorted quartz sandstone at the base, transitioning to lacustrine shale at the top.

The extensional phase at this stage plays an important role in controlling the geometry of the basin, resulting in the characteristics of transgressional deposits or environmental changes from non-marine to the Outer Neritic environment. The transgression phase is good in the formation of source rock, so it is possible that the Lower Cibulakan Marker could become a source rock, and the quality will be discussed in the next paragraph. Furthermore, at the final stage of this phase, the rise in sea level will be deposited in the Middle Cibulakan Marker. This marker is a carbonate platform composed of clastic limestone at the lower part and a pinnacle reef at the upper part (Fig. 14c). The final section shows characteristics of regressional deposits, possibly the last extensional phase in the Middle Miocene had begun to stop, and the high sediment supply in the basin produced regressional sedimentary rocks of Upper Cibulakan Marker.

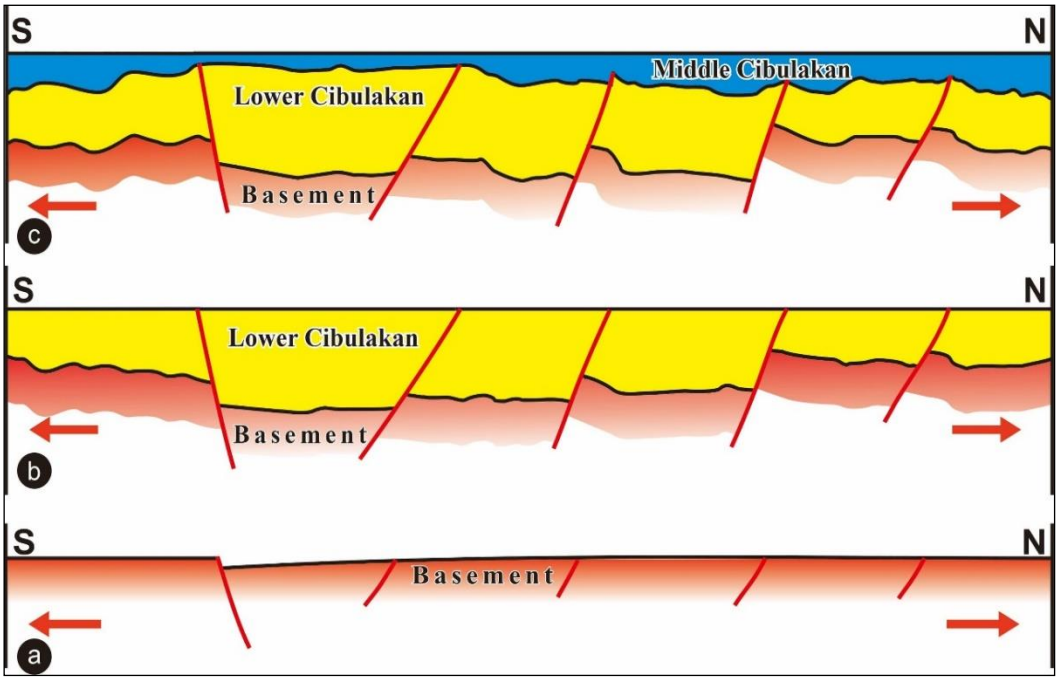


Fig. 14. Geohistory model of the Early Miocene to Middle Miocene age: (a) The extensional pre-rift basement phase will produce normal fault traces and open up sedimentation accommodation space; (b) Basin filling by Lower Cibulakan sediment in half-graben; (c) Deposition of Middle Cibulakan Markers due to transgression phase in the form of platform carbonate and pinnacle reef

4.3.2. Middle Miocene-Late Miocene

Starting from the Upper Cibulakan Marker, formed in the Middle Neritic environment, until the Parigi Marker in the Middle–Inner Neritic environment. The characteristics of the regressive deposits indicate the influence of compressional tectonic processes, which cause the basin uplift process (Fig. 15a). Major faults in the southern part developed synthetic faults, which offset the forces caused by the thickening of sedimentation in this section. This will continue until the deposition of the Upper Cibulakan Marker with shale facies is finished. The Parigi Marker was deposited in this phase as clastic limestone facies due to rising sea levels. The thickening of limestone facies occurs in the middle due to the loading process and the addition of pressure. After the deposition of the Parigi Marker ended, there was a change in the main stress style to north-south trending compression (Fig. 15b).

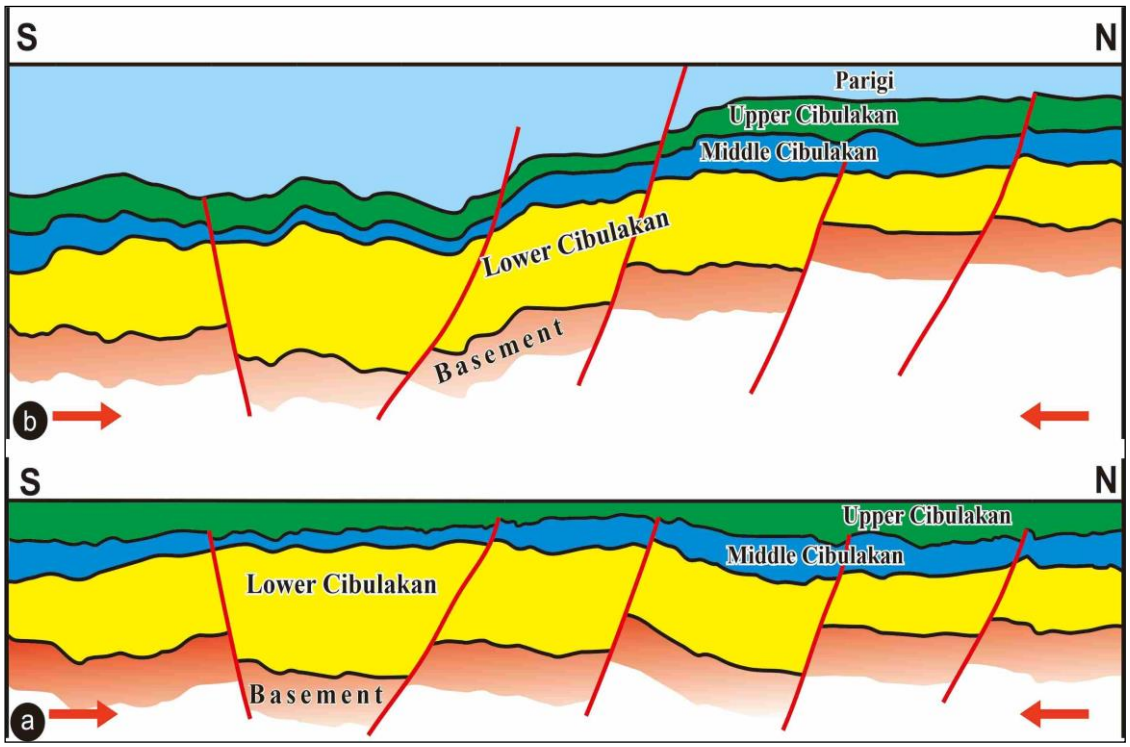


Fig. 15. Geohistory model of the Middle Eocene to Late Eocene age: a) Compression tectonics produce transgressive sediments from the Upper Cibulakan Marker; b) The loading process results in the thickening of the layer in the middle and is characterized by vertical elongation of the fault

4.3.3. Late Miocene-Late Pliocene

A continuation of the previous compression phase but with a higher intensity causes the increase of the thrust fault in the southern part and the centre of the basin in the northern part to experience subsidence, with the result of a transgressional lithologic group of the lower Cisubuh Marker in the Middle Neritic environment (Fig. 16a). Similar to the initial phase (Early Miocene), this phase is also interpreted to form source rocks with shallow marine characteristics. At the final stage of this phase, with the compression intensity having stopped and volcanic activity increasing in the southern arc of this basin, a regressional succession of the Intra Cisubuh, Upper Cisubuh Markers and Damar Formation (Fig. 16b, 16c, and 16d). The Damar formation's characteristics are volcaniclastic rocks in the Inner Neritic to Non-Marine environment due to increased volcanic activity in the Javanese volcanic area, which will continue to fill in until the basin is closed.

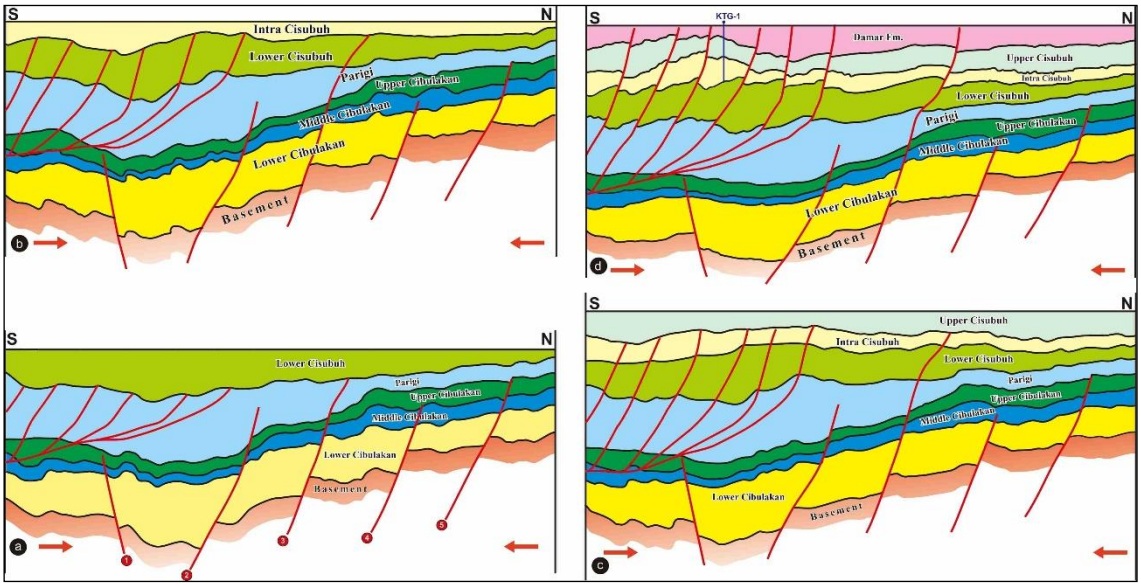


Fig. 16. Geohistory model of the Late Miocene to Late Pliocene age: a) sedimentation of the lower Cisubuh Marker as a product of phase regression; b) the regression phase continues with the deposition of the Intra Cisubuh Marker; c and d) the Upper Cisubuh Marker and volcaniclastic rocks are the last sediments deposited during the compression process

4.4. Hydrocarbon Trapping Mechanism

Starting from the hydrocarbon generation process in the lower layers of the Lower Cibulakan Marker, which is composed of shale lithology, the results of the geochemical analysis show that this shale is rich in organic material and is a good source rock for producing hydrocarbons. Based on the drilling of the NCJ-B1 well, this shale has a Total Organic Carbon (TOC) ranging from 0.83% -1.66%. The Tmax resulting from this analysis is around 420 °C. The Potential Yield (PY) value is around 0.95-8.36 kg/ton, and the Hydrocarbon Index is around 98-466. Under these conditions, the shale of the Lower Cibulakan Marker can act as a source rock so that hydrocarbons can be generated. The hydrocarbon generation process is followed by vertical migration through normal faults connecting the kitchen area to overlying formations. This vertical migration process will be followed by lateral migration, which will move hydrocarbons through the pores in the reservoir rock.

The movement of hydrocarbon fluid will fill the traps in the reservoir rock. Reservoirs are identified in the Kendal Sub-basin: sandstone of Lower Cibulakan, limestone of Middle Cibulakan, limestone of Parigi, and sandstone of Intra Cisubuh. The sandstone of Lower Cibulakan has good reservoir properties, showing a high porosity value of around 22%. Then, the limestone of Middle Cibulakan developed as clastic rocks and carbonate reefs with an average porosity of 18%. The limestone reservoir of Parigi, developed as a carbonate reef outcrop, occupies relatively high areas and is limited by thrust faults. The porosity that develops in this formation is around 14%. Meanwhile, the sandstone reservoir of Intra Cisubuh is widespread in the Kendal Sub-basin area, with a porosity value of 22%. Play model analysis shows that the hydrocarbon traps that develop in the research area can generally be divided into structural and stratigraphic traps. Structural traps include thrust anticline, sub-thrust, horst block, and fold on downthrown normal fault block. Meanwhile, stratigraphic traps are dominated by pinch-out sand and built-up carbonate (Fig. 17). These hydrocarbon traps are spread across all parts of the sub-basin with a relatively small size. This trap will generate economic value with an estimated total recoverable resource of 112.12 MMBO and 14.16 BSCF with a recovery factor of 35% (Table 2). By seeing this economic value, the right exploration method is needed in the development of oil and gas fields in the future.

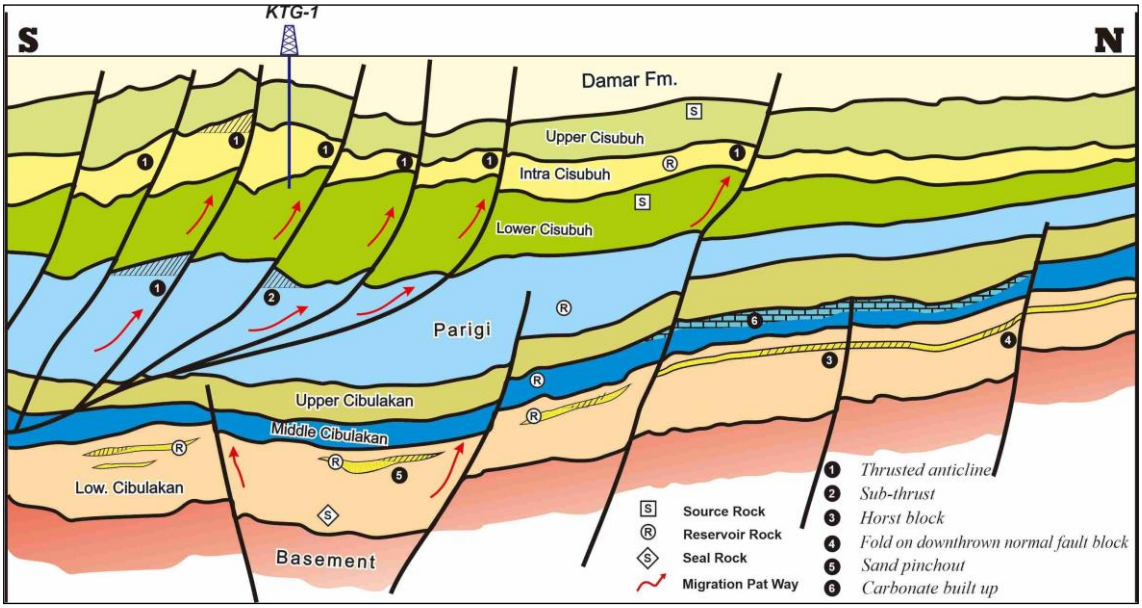


Fig. 17. Model and mechanism of hydrocarbon trapping in the Kendal sub-basin. Hydrocarbon migration starts from the kitchen area through faults and fills structural and stratigraphic traps

Table 2. Estimation of total hydrocarbon resources

Marker	OOIP (MMBO)	Rec. Resources (MMBO)	OGIP (BSCF)	Rec. Resources (MMBO)
Lower Cibulakan	166.16	58.16	-	-
Intra Cisubuh	154.16	53.96	-	-
Middle Cibulakan	-	-	6.30	4.41
Parigi	-	-	13.93	9.75
TOTAL	320.32	112.12	20.23	14.16

5. Conclusions

The Kendal Sub-basin's geological structure is shaped by three key tectonic phases. The Early to Middle Miocene rifting phase formed a half-graben structure, providing accommodation space for source rock deposition. Subsequent Middle to Late Miocene compression led to the uplift and deformation of basin-fill sequences, influencing reservoir and trap formation. The final phase, from the Late Miocene to the Late Pliocene, involved intensified thrust faulting, which enhanced structural trap development.

Hydrocarbon generation occurs within the Lower Cibulakan shale, with migration facilitated by normal and thrust faults. Structural traps, including thrust anticlines and horst blocks, dominate the basin, while stratigraphic traps are primarily represented by pinch-out sands and carbonate buildups. The integration of surface and subsurface data in this study provides valuable insights into the hydrocarbon potential of this underexplored basin, offering significant implications for future exploration efforts in the research area.

Acknowledgments

The authors would like to thank the data and information centre (PUSDATIN) of the Ministry of Energy and Mineral Resources for the permission to use subsurface data.

References

Abd, O.K., Abd, N., 2023. 2D seismic structural interpretation of Yamama Formation in Al-Fao area, Basrah, Iraq. Iraqi Geological Journal, 56(2), 304-313. https://doi.org/10.46717/igj.56.2E.21ms-2023-11-26.

Adha, I., 2021. Karakteristik batuan formasi Kerek sebagai reservoir di lapangan Cipluk Kendal. Petrogas: Journal of Energy and Technology, 3(2), 39-50. https://doi.org/10.58267/petrogas.v3i2.69.

Alencar, M.L., Miranda, T.S.de, Correia Filho, O.J., Barbosa, J.A., Gomes, I.F., Silva Ramos, G.M., Araújo, A.F.L.de, Topan, J.G. deO., Celestino, M.A.L., Neumann, V.H., 2024. The effect of fracture networks on the vertical permeability of a tight carbonate reservoir analogue: laminites from the Crato Formation, NE Brazil. Marine and Petroleum Geology, 162, 106735. https://doi.org/10.1016/j.marpetgeo.2024.106735.

Ângelo da Silva Neto, C., Rodrigues do Nascimento Junior, D., Duarte, C.R., Freires, E.V., Leopoldino Oliveira, K.M., Ibanez, D.M., Pestilho, A.L.S., Miranda, F.P., Penteado, H.L.B., Dias Filho, D.C., Viveen, W., Baby, P., Hurtado-Enríquez, C., Meixner, J., Grimmer, J.C., Becker, A., Schill, E., Kohl, T., Ranjbari, M.R., Więsek, M., 2021. Assessing the accuracy of combined DEM-based lineament mapping and the normalised SL-index as a tool for active fault mapping. Journal of South American Earth Sciences, 71, 256-268. https://doi.org/10.1016/j.tecto.2021.228942.

Aribowo, S., Husson, L., Natawidjaja, D.H., Authemayou, C., Daryono, M.R., Puji, A.R., Valla, P.G., Pamumpuni, A., Wardhana, D.D., de Gelder, G., Djarwadi, D., Lorcery, M., 2022. Active back-arc thrust in North West Java, Indonesia. Tectonics, 41(7). https://doi.org/10.1029/2021TC007120.

Audithia, W., Awari, S., Wiyono, J., 2016. New consideration for petroleum system implications of the Late Miocene reservoir in the North Serayu Basin, Central Java. Proceeding of Indonesian Petroleum Association, 85(1), 6. https://doi.org/10.29118/ipa.0.16.150.g.

Badawi, D., Gildin, E., 2025. Neural operator-based proxy for reservoir simulations considering varying well settings, locations, and permeability fields. Computers and Geosciences 196 (July 2024). https://doi.org/10.1016/j.cageo.2024.105826.

Betzler, C., Hübscher, C., Lindhorst, S., Lüdmann, T., Hincke, C., Beaman, R.J., Webster, J.M., 2024. Seismic stratigraphic and sedimentary record of a partial carbonate platform drowning, Queensland Plateau, north-east Australia. Marine Geology, 470, 107255. https://doi.org/10.1016/j.margeo.2024.107255.

Camanni, G., Vinci, F., Tavani, S., Ferrandino, V., Mazzoli, S., Corradetti, A., Parente, M., Iannace, A., 2021. Fracture density variations within a reservoir-scale normal fault zone: A case study from shallow-water carbonates of southern Italy. Journal of Structural Geology, 151, 104432. https://doi.org/10.1016/j.jsg.2021.104432.

Feng, Y.W., Qu, H.J., Zhang, G.C., Pu, R.H., 2017. Seismic interpretation and hydrocarbon accumulations implication of the Miocene Meishan Formation reefs in southern Qiongdongnan Basin, northern South China Sea. Journal of Palaeogeography, 6 (3), 206–218. https://doi.org/10.1016/j.jop.2017.05.002.

Giao, P.H., Hien, D.H., Trang, P.H., Ngoc, P.Q., Dung, B.V., Man, H.Q., 2025. An innovative seismo-petrophysical characterization of a turbidite sand in the Nam Con Son Basin, using permeability-linked adaptive rock physics template (K-ARPT) with reference to gas exploration and carbon storage. Marine and Petroleum Geology, 173, 107263. https://doi.org/10.1016/j.marpetgeo.2024.107263.

Gunawan, E., Widiyantoro, S., 2019. Active tectonic deformation in Java, Indonesia inferred from a GPS-derived strain rate. Journal of Geodynamics, 123, 49–54. https://doi.org/10.1016/j.jog.2019.01.004.

Harding, T.P., 1985. Seismic characteristics and identification of negative flower structures, positive flower structures, and positive structural inversion. American Association of Petroleum Geologists Bulletin, 69(4), 582–600. https://doi.org/10.1306/ad462538-16f7-11d7-8645000102c1865d.

Harzali, M., Troudi, H., Ben Boubaker, K., Ouali, J., 2014. Carbonate platform-margins and reefs distribution using 2-D seismic analysis, Central Tunisia. Journal of African Earth Sciences, 100, 109–120. https://doi.org/10.1016/j.jafrearsci.2014.06.007.

Heriawan, M.N., Syafi'i, A.A., Saepuloh, A., Kubo, T., Koike, K., 2021. Detection of near-surface permeable zones based on spatial correlation between radon gas concentration and DTM-derived lineament density. Natural Resources Research, 30 (4), 2989–3015. https://doi.org/10.1007/s11053-020-09718-z.

Husein, S., Jyalita, J., Nursecha, M.A.Q., 2013. Kendali stratigrafi dan struktur gravitasi pada rembesan hidrokarbon sijenggung, cekungan serayu utara. Prosiding Seminar Nasional Kebumian Ke-6, 12, 474–489.

Irsyam, M., Cummins, P.R., Asrurifak, M., Faizal, L., Natawidjaja, D.H., Widiyantoro, S., Meilano, I., Triyoso, W., Rudiyanto, A., Hidayati, S., Ridwan, M., Hanifa, N.R., Syahbana, A.J., 2020. Development of the 2017 national seismic hazard maps of Indonesia. Earthquake Spectra, 36(1), 112–136. https://doi.org/10.1177/8755293020951206.

Jamal, J., Sanjaya, I., Saputro, D.H., Suteja, A., 2024. Geological structures in the formation of the kendal plains: insights from remote sensing imagery. Jurnal Geologi Dan Sumberdaya Mineral, 25(4), 217–223. https://doi.org/10.33332/jgsm.geologi.v25i4.827.

Kurniasih, A., Kusumawijaya, E., Ferdy, F., Fahrudin, F., Setyawan, R., 2021. Biostratigraphy analysis of barbatos-1 exploration well in tomori block, Banggai basin, east Arm of Sulawesi. RISET Geologi Dan Pertambangan, 31(1), 51-62. https://doi.org/10.14203/risetgeotam2021.v31.1150.

Li, B., Zhao, S., Liu, Y., Yang, X., Liu, Y., Zhang, J., Zhang, C., Li, J., Wang, G., Yin, M., 2024. Fracture features and fault influence on gas accumulation in the Longmaxi Formation in Changning block, southern Sichuan Basin. Natural Gas Industry B, 11(5), 482–495. https://doi.org/10.1016/j.ngib.2024.09.007.

Logan, G.A., Jones, A.T., Kennard, J.M., Ryan, G.J., Rollet, N., 2010. Australian offshore natural hydrocarbon seepage studies, a review and re-evaluation. Marine and Petroleum Geology, 27(1), 26–45. https://doi.org/10.1016/j.marpetgeo.2009.07.002.

Majumdar, T.J., Bhattacharya, B.B., 1988. Application of the haar transform for extraction of linear and anomalous patterns over part of Cambay Basin, India. International Journal of Remote Sensing, 9(12), 1937–1942. https://doi.org/10.1080/01431168808954992.

Meixner, J., Grimmer, J.C., Becker, A., Schill, E., Kohl, T., 2018. Comparison of different digital elevation models and satellite imagery for lineament analysis: Implications for identification and spatial arrangement of fault zones in crystalline basement rocks of the southern Black Forest (Germany). Journal of Structural Geology, 108, 256–268. https://doi.org/10.1016/j.jsg.2017.11.006.

Mendes, L. de C., Basso, M., Villacreces Morales, J., Chinelatto, G.F., Blanco, J.M., Correia, U.M.C., Ponte, J.P., Matheus, G.F., Camargo, M.M., Gavidia, J.C.R., Medeiros, R.S.P. d., Vidal, A.C., 2024. The influence of major faults and fractures on the development of non-matrix porosity system in a pre-salt carbonate reservoir, Santos Basin – Brazil. Journal of Structural Geology, 189, 105271. https://doi.org/10.1016/j.jsg.2024.105271.

Moura Costa, F., Tavares Melo, A., Amâncio Novo, T., 2023. Three-dimensional characterization of the Búzios Field reveals implications on the tectonostratigraphic evolution of the Santos Basin using combined seismic attributes and well-logs analysis. Journal of South American Earth Sciences, 131, 104541. https://doi.org/10.1016/j.jsames.2023.104541.

Nabawy, B.S., Mostafa, A., Radwan, A.A., Kotb, A.G., Leila, M., 2023. Seismic reservoir characterization of the syn-rift Lower Miocene Rudeis Formation in the July oilfield, Gulf of Suez basin, Egypt: Implication for reservoir quality assessment. Geoenergy Science and Engineering, 226, 211797. https://doi.org/10.1016/j.geoen.2023.211797.

Novianto, A., Sutanto, S., Suharsono, S., Prasetyadi, C., Setiawan, J., 2022. Structure boundary separating using gravity data for central and southern parts of the east Java basin beneath the Quaternary volcanic deposits. Iraqi Geological Journal, 55(1), 1–13. https://doi.org/10.46717/igj.55.1B.1Ms-2022-02-17.

Nursecha, M., Jyalita, J., Husein, S., 2014. Tectonic control on hydrocarbon seepages of sijenggung, north Serayu basin, central Java. Proceeding of Indonesian Petroleum Association, IPA14-SG-021.

Pasari, S., Simanjuntak, A.V.H., Mehta, A., Neha, Sharma, Y., 2021. The current state of earthquake potential on Java Island, Indonesia. Pure and Applied Geophysics, 178(8), 2789–2806. https://doi.org/10.1007/s00024-021-02781-4.

Praptisih, P., 2016. Karakteristik batuan induk hidrokarbon dan hubungannya dengan rembesan minyak di lapangan minyak cipluk, kabupaten kendal, provinsi Jawa Tengah. Buletin Sumber Daya Geologi, 11(2), 133–143. https://doi.org/10.47599/bsdg.v11i2.26.

Romario, I.F.B., Suprapto, R., Pambudi, D., Chandra, R., Pratama, I., Fauzan, M., R, P., Rachman, R., 2016. Studi paleogeografi neogen batas cekungan kendeng-serayu utara: tantangan dan implikasi pada konsep eksplorasi minyak dan gas bumi di tinggian semarang regional Jawa Tengah bagian utara. Proceeding, Seminar Nasional Kebumian Ke-9, 115–126.

Satyana, A.H., 2005. Structural indentation of central Java: a regional wrench segmentation. Proceeding Joint Convention Surabaya 2005 — HAGI-IAGI-PERHAPI, JCS2005-V0 (1), 193–204.

Satyana, A.H., 2007. Central Java new considerations on the tectonic evolution and petroleum. Proceedings of the Thirty- First Annual Convention, (Jakarta: Indonesian Petroleum Association). Indonesian Petroleum Association, IPA07-G-085.

Sharaf, E.F., Sheikha, H., 2021. Reservoir characterization and production history matching of Lower Cretaceous, Muddy formation in Ranch Creek area, Bell Creek oil field, southeastern Montana, USA. Marine and Petroleum Geology, 127, 104996. https://doi.org/10.1016/j.marpetgeo.2021.104996.

Simandjuntak, T.O., Barber, A.J., 1996. Contrasting tectonic styles in the neogene orogenic belts of Indonesia. Geological Society Special Publication, 106, 185–201. https://doi.org/10.1144/GSL.SP.1996.106.01.12.

Sribudiyani, S., Muchsin, N., Ryacudu, R., Kunto, T., Astono, P., 2003. The collision of the east Java microplate and its implication for hydrocarbon occurrences in the east Java basin. Proceedings of the Twenty-Ninth Annual Convention, (Jakarta: Indonesian Petroleum Association). https://doi.org/10.29118/ipa.1530.03.g.085.

Syaeful, H., Sukadana, I.G., Indrastomo, F.D., Rachael, Y., Ciputra, R.C., Adimedha, T.B., Pratiwi, F., Rosianna, I., Yuliastuti, Cakrabuana, W., Faizah, Y., Santoso, E., Sudrajat, A., Zakaria, Z., 2024. Near regional geology of Pantai Gosong NPP Site, West Kalimantan, Indonesia: Capable fault and geotechnical hazards assessment. Nuclear Engineering and Design, 423, 113207. https://doi.org/10.1016/j.nucengdes.2024.113207.

Thaden, R.E., Sumadirdja, H., Richards, P.W., 1975. Geologic Map of the Magelang and Semarang Quadrangles, Java.

Wang, X., Jiang, F., Zheng, X., Chen, D., Qi, Z., Liu, Y., Guo, J., Zhang, Y., 2024. Source rock evaluation and hydrocarbon expulsion characteristics of effective source rocks in the Fushan depression, Beibuwan basin, China. Minerals, 14(10), 1-34. https://doi.org/10.3390/min14100975.

Wilson, M.E.J., Hall, R., 2010. Tectonic influences on SE Asian carbonate systems and their reservoir development. Cenozoic Carbonate Systems of Australasia, 95, 13–40. https://doi.org/10.2110/sepmsp.095.013.

Xu, Y., Ren, J., 2025. Consequences of preexisting faults on rifting patterns: Insights from multichannel seismic data of the Shunde rift, Northern South China Sea. Journal of Structural Geology, 191, 105331. https://doi.org/10.1016/j.jsg.2024.105331.

Zhang, J., Cao, J., Wang, Y., Li, J., Hu, G., Zhou, N., Shi, T., 2019. Geochemistry and genesis of oil and gas seeps in the Junggar basin, NW China: Implications for Hybrid Petroleum Systems. Geofluids, 2019, 1-26. https://doi.org/10.1155/2019/9732674.

Zhu, H., Wang, Y., Choi, B. Do, Pan, Y., 2025. Ostracod fauna from the Lower Cretaceous Jingchuan Formation of Ordos basin in China and its biostratigraphic significance. Cretaceous Research, 168, 106068. https://doi.org/10.1016/j.cretres.2024.106068.